12

Tensor Invariants and their Gradients

Gordon Kindlmann

School of Computing, University of Utah, 50 South Central Campus Drive, Salt Lake City, UT 84112, USA
gk@cs.utah.edu

Summary. Second-order tensors may be described in terms of *shape* and *orientation*. Shape is quantified by tensor *invariants*, which are fixed with respect to coordinate system changes. This chapter describes an anatomically-motivated method of detecting edges in diffusion tensor fields based on the *gradients* of invariants. Three particular invariants (the mean, variance, and skewness of the tensor eigenvalues) are described in two ways: first, as the geometric parameters of an intuitive graphical device for representing tensor shape (the *eigenvalue wheel*), and second, in terms of their physical and anatomical significance in diffusion tensor MRI. Tensor-valued gradients of these invariants lead to an orthonormal basis for describing changes in tensor shape. The spatial gradient of the diffusion tensor field may be projected onto this basis, producing three different measures of edge strength, selective for different kinds of anatomical boundaries. The gradient measures are grounded in standard tensor analysis, and are demonstrated on synthetic data.

12.1 Background and Notation

As described in Chap. 5 by Alexander, fields of water diffusion tensors may be measured *in vivo* with magnetic resonance imaging (MRI), providing a valuable tool for assessing the organization of tissue microstructure. A diffusion tensor $\mathbf{D}$ is numerically estimated by its matrix representation in the orthonormal *laboratory frame* $\mathcal{L} = \{\mathbf{b}_1, \mathbf{b}_2, \mathbf{b}_3\}$ associated with the MRI scanner [1]:

$$[\mathbf{D}]_{\mathcal{L}} = \begin{bmatrix} D_{11} & D_{12} & D_{13} \\ D_{12} & D_{22} & D_{23} \\ D_{13} & D_{23} & D_{33} \end{bmatrix} .$$

Unit-length eigenvectors $\mathbf{e}_i$ can be found to form an orthonormal *principal frame* $\mathcal{E} = \{\mathbf{e}_1, \mathbf{e}_2, \mathbf{e}_3\}$, in which the matrix representation of $\mathbf{D}$ has the eigenvalues λ_i along the diagonal:

$$[\mathbf{D}]_{\mathcal{E}} = \begin{bmatrix} \lambda_1 & 0 & 0 \\ 0 & \lambda_2 & 0 \\ 0 & 0 & \lambda_3 \end{bmatrix} \Rightarrow [\mathbf{D}]_{\mathcal{L}} = R \begin{bmatrix} \lambda_1 & 0 & 0 \\ 0 & \lambda_2 & 0 \\ 0 & 0 & \lambda_3 \end{bmatrix} R^{\mathsf{t}} .$$

Column i of rotation matrix R is unit-length eigenvector representation $[\mathbf{e}_i]_{\mathcal{L}}$. Diagonalizing a matrix representation of $\mathbf{D}$ into eigenvalues and eigenvectors separates the tensor into shape and orientation information, respectively. Herein, tensor 'shape' refers to the unordered set of three eigenvalues.

12.2 From Principal Invariants to Eigenvalues

The eigenvalues of a symmetric tensor $\mathbf{D}$ are computed by solving its cubic characteristic polynomial:

$$\det(\lambda\mathbf{I} - \mathbf{D}) = 0$$

The determinant of $\lambda\mathbf{I} - \mathbf{D}$ may be computed in the laboratory frame:

$$\det(\lambda I - [\mathbf{D}]_{\mathcal{L}}) = \begin{vmatrix} \lambda - D_{11} & -D_{12} & -D_{13} \\ -D_{12} & \lambda - D_{22} & -D_{23} \\ -D_{13} & -D_{23} & \lambda - D_{33} \end{vmatrix} = \lambda^3 - J_1\lambda^2 + J_2\lambda - J_3 \ ;$$

$$\begin{aligned} J_1 &= D_{11} + D_{22} + D_{33} \\ J_2 &= D_{11}D_{22} + D_{11}D_{33} + D_{22}D_{33} - D_{12}^2 - D_{13}^2 - D_{23}^2 \\ J_3 &= 2D_{12}D_{13}D_{23} + D_{11}D_{22}D_{33} - D_{13}^2D_{22} - D_{11}D_{23}^2 - D_{12}^2D_{33} \end{aligned} \tag{12.1}$$

On the other hand, evaluating $\det(\lambda\mathbf{I} - \mathbf{D})$ in the principal frame $\mathcal{E}$ gives:

$$J_1 = \lambda_1 + \lambda_2 + \lambda_3 \ ; \ J_2 = \lambda_1\lambda_2 + \lambda_1\lambda_3 + \lambda_2\lambda_3 \ ; \ J_3 = \lambda_1\lambda_2\lambda_3 \tag{12.2}$$

J_1, J_2, J_3 are the *principal invariants* [2], with coordinate free expression:

$$J_1 = \mathrm{tr}(\mathbf{D}) \ ; \ J_2 = \frac{\mathrm{tr}(\mathbf{D})^2 - \mathrm{tr}(\mathbf{D}^2)}{2} \ ; \ J_3 = \det(\mathbf{D}) \tag{12.3}$$

Equation (12.1) is how the principal invariants are computed in practice, based on the matrix components of the tensor represented in the laboratory frame. Equation (12.2) shows how J_i are functions of λ_i alone.

Another useful invariant J_4 is computed from the principal invariants:

$$\begin{aligned} J_4 = \mathrm{tr}(\mathbf{D}^{\mathbf{t}}\mathbf{D}) &= J_1^2 - 2J_2 \\ &= D_{11}^2 + 2D_{12}^2 + 2D_{13}^2 + D_{22}^2 + 2D_{23}^2 + D_{33}^2 \\ &= \lambda_1^2 + \lambda_2^2 + \lambda_3^2 \end{aligned}$$

J_1 and J_4 both describe tensor *size*, either by the sum of the eigenvalues, or their squares, respectively. Much of the DT-MRI literature has noted the utility of the J_i invariants as measures of tensor shape that do not require diagonalization [1, 3, 4]. Computing eigenvalues, however, is simply arithmetic combination of principal invariants to create new invariants. The standard formulas for solving cubic polynomials define [5, 6]:

$$Q = \frac{J_1^2 - 3J_2}{9} \; ; \; R = \frac{-9J_1J_2 + 27J_3 + 2J_1^3}{54} \; ; \; \Theta = \frac{1}{3}\cos^{-1}\left(\frac{R}{\sqrt{Q^3}}\right) \quad (12.4)$$

With these, the three eigenvalues (themselves invariants) are:

$$\begin{aligned} \lambda_1 &= J_1/3 + 2\sqrt{Q}\cos(\Theta) \\ \lambda_2 &= J_1/3 + 2\sqrt{Q}\cos(\Theta - 2\pi/3) \\ \lambda_3 &= J_1/3 + 2\sqrt{Q}\cos(\Theta + 2\pi/3) \end{aligned} \quad (12.5)$$

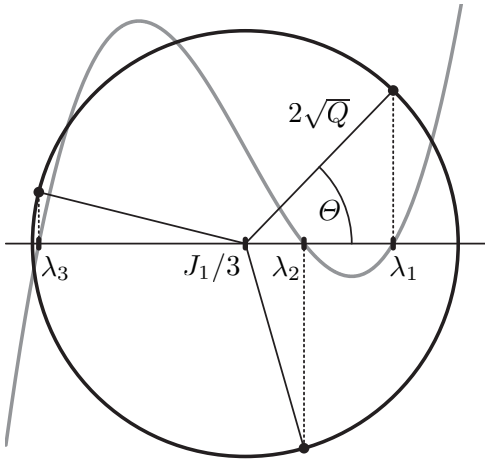

Fig. 12.1. Characteristic polynomial in gray, eigenvalues λ_i, and wheel parameters J_1, Q, Θ

12.3 Eigenvalue Wheel

The structure of (12.5) suggests a geometric analogy, shown in Fig. 12.1 [7]. A wheel with three equally placed spokes is centered on the real number line at $J_1/3$. The radius of the wheel is $2\sqrt{Q}$, and Θ measures the orientation. The eigenvalues are the projection of the spoke ends onto the horizontal axis. The wheel geometry can be expressed in terms of statistics of the unsorted eigenvalues, starting with their *central moments* μ_1, μ_2, μ_3:

$$\begin{aligned} \mu_1 &= \langle \lambda_i \rangle = J_1/3 \\ \mu_2 &= \langle (\lambda_i - \mu_1)^2 \rangle = 2Q \\ \mu_3 &= \langle (\lambda_i - \mu_1)^3 \rangle = 2R \end{aligned} \quad (12.6)$$

The eigenvalue mean, variance and standard deviation are μ_1, μ_2, and $\sigma = \sqrt{\mu_2}$, respectively. The skewness of the eigenvalues α_3 is defined as [5][1]:

[1] 'Skewness' can also refer to μ_3, as in Chap. 5.

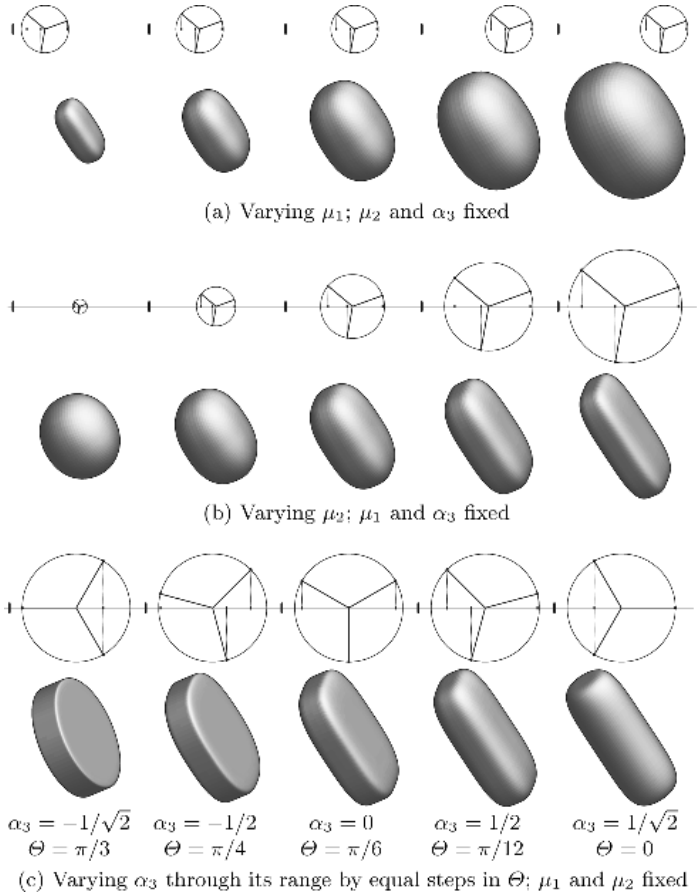

Fig. 12.2. Visualizations of shape variations associated with changing eigenvalue mean μ_1 (wheel location), variance μ_2 (wheel radius) and skewness α_3 (spoke angle)

$$\alpha_3 = \frac{\mu_3}{\sigma^3} = \frac{R}{\sqrt{2Q^3}} = \frac{\cos(3\Theta)}{\sqrt{2}} \;\Rightarrow\; \Theta = \frac{1}{3}\cos^{-1}(\sqrt{2}\,\alpha_3) \tag{12.7}$$

Note that the eigenvalue statistics determine the wheel parameters. The *geometric* intuition that the wheel's location, radius, and orientation may be varied in isolation is grounded in the *statistical* property that mean, variance, and skewness are orthogonal. That is, viewing μ_1, μ_2, and α_3 as scalar functions over the space of unsorted eigenvalue triples $(\lambda_1, \lambda_2, \lambda_3)$, and letting $\nabla_\lambda J$ be the gradient of scalar invariant J over $(\lambda_1, \lambda_2, \lambda_3)$, one finds:

$$\nabla_\lambda \mu_1 \cdot \nabla_\lambda \mu_2 = 0 \;;\; \nabla_\lambda \mu_1 \cdot \nabla_\lambda \alpha_3 = 0 \;;\; \nabla_\lambda \mu_2 \cdot \nabla_\lambda \alpha_3 = 0 \;. \tag{12.8}$$

The orthogonality of μ_1, μ_2, α_3 was described by Bahn [8] with cylindrical coordinates for $(\lambda_1, \lambda_2, \lambda_3)$ space. Previous work in continuum mechanics defined related orthogonal measures with the mean, variance, and skewness of the logarithms of the strain tensor eigenvalues [9]. Figure 12.2 illustrates the orthogonal invariants with eigenvalue wheels and superquadric glyphs [10].

12.4 Anatomical Significance of Eigenvalue Statistics

The measures described in the previous sections take on physical meaning when interpreted in the context of a particular application domain, such as diffusion tensor imaging. The diffusion tensor eigenvalues are the apparent diffusion coefficients (ADCs) along the eigenvectors [1]. Eigenvalue mean μ_1 is the *bulk mean diffusivity* [11], the average of ADC over all possible directions. This readily distinguishes the cerebral spinal fluid (CSF) of the ventricles (high μ_1) from the white and gray matter (lower μ_1). An important empirical fact is that μ_1 is essentially constant across white and gray matter [11, 12, 13]. Isolating this degree of freedom permits μ_2 and α_3 to better characterize the brain tissue features that DT-MRI is uniquely capable of detecting.

The variance of the eigenvalues μ_2 measures the directional dependence of the ADC, which indicates anisotropic microstructure. As described in Chap. 5, anisotropy is generally low in gray matter, and high in white matter, due in part to myelinated axon sheaths [14]. Basser and Pierpaoli defined the *fractional* and *relative* anisotropy measures with μ_2 [15]:

$$\mathrm{FA} = \sqrt{\frac{3}{2}}\frac{\|\mathbf{D}-\mu_1\mathbf{I}\|}{\|\mathbf{D}\|} = 3\sqrt{\frac{\mu_2}{2J_4}}\ ;\ \mathrm{RA} = \frac{\|\mathbf{D}-\mu_1\mathbf{I}\|}{\|\mu_1\mathbf{I}\|} = \sqrt{\frac{\mu_2}{\mu_1^2}}\ . \tag{12.9}$$

The empirical constancy of μ_1 in brain tissue helps compensate for the unfortunate property (visible in Fig. 12.2(a)) that varying μ_1 separately from μ_2 and α_3 effectively changes the anisotropy defined by FA or RA. This assumes, however, that CSF can be masked out with μ_1, which can be somewhat challenging given the limited spatial resolution of DT-MRI.

Eigenvalue skewness α_3 isolates the variation between anisotropic tensors which are 'planar' (large in two axes and small in the other) versus 'linear' (large along one axis, small in the others). This shape variation is not measured by the usual anisotropy metrics: from (12.8) and (12.9), skewness is in fact *orthogonal* to FA and RA. There are two related aspects to the anatomical significance of eigenvalue skewness. The phenomenon of *partial voluming* is a basic characteristics of discretely sampled medical images, in which the sample value records a measurement over some spatial extent related to the spacing between samples. Previous analysis of partial voluming in DT-MRI demonstrated a bias towards planar anisotropy caused by measurement mixing of adjacent regions of linear anisotropy along orthogonal orientations [16, 17]. Planar anisotropy can also arise in more complex configurations. For example, previous work in visualizing regions of significant planar anisotropy characterized locations where populations of differently-oriented fibers apparently mix at a fine scale, far below that of the image resolution [18]. A location with this configuration is the intersection of the medial-lateral tracts of the corpus callosum and inferior-superior tracts of the corona radiata, as confirmed by high-angular resolution diffusion imaging in [19].

12.5 Edge Detection with Invariant Gradients

One strategy for image processing on diffusion tensor data is to locally decompose the space of tensor values (at each tensor sample) into shape changes and orientation changes, enabling a more anatomically driven approach to edge and feature detection. Measuring spatial changes in eigenvalue mean μ_1 could isolate the boundary of the cerebral spinal fluid. Rapid changes in μ_2 might indicate the transition from gray matter to white matter, as well as structural variations within white matter. Changes in α_3 might signal the partial voluming between regions of orthogonally oriented white matter structures. In all cases, disregarding changes in tensor *orientation* may reduce the chance of falsely identifying structural boundaries. Implementing this strategy involves the *gradients* of eigenvalue statistics. This generalizes previous work decomposing tensor changes into changes in the isotropic component, and changes in anisotropy and orientation (the deviator) [20].

Some elements of tensor analysis are reviewed herein [2]. Though a diffusion tensor $\mathbf{D}$ is often identified with its matrix components in the laboratory frame, $\mathbf{D}$ is in fact an element of $L(\mathbb{R}^3, \mathbb{R}^3)$, the set of linear transforms from $\mathbb{R}^3$ to $\mathbb{R}^3$ (see Chap. 1 by Hagen and Garth). $L(\mathbb{R}^3, \mathbb{R}^3)$ is a vector space [21], so every tensor *is* also a vector. Though potentially confusing, recognizing $L(\mathbb{R}^3, \mathbb{R}^3)$ as a vector space grounds the tensor analysis below on our geometric intuition about bases, projections, and gradients from vector calculus. The double contraction $\mathbf{C}:\mathbf{D} = \mathrm{tr}(\mathbf{C}^{\mathrm{t}}\mathbf{D})$ endows $L(\mathbb{R}^3, \mathbb{R}^3)$ with an inner (or dot) product. The tensor norm is defined as $\|\mathbf{D}\| = \sqrt{\mathbf{D}:\mathbf{D}}$. The tensor product of vectors $\mathbf{u}\otimes\mathbf{v}$ is defined by $(\mathbf{u}\otimes\mathbf{v})\mathbf{x} = \mathbf{u}(\mathbf{v}\cdot\mathbf{x})$ for all vectors $\mathbf{x}$. The Kronecker delta δ_{ij} is 1 if $i = j$ and 0 otherwise. The coordinate-free *spectral decomposition* of a symmetric tensor $\mathbf{D}$ into eigenvalues and unit-length eigenvectors is:

$$\mathbf{D} = \textstyle\sum_i \lambda_i \mathbf{e}_i \otimes \mathbf{e}_i \tag{12.10}$$

Just as invariants characterize tensor shape, gradients of invariants characterize changes in tensor shape. Herein, 'invariant gradient' denotes differentiation with respect to the tensor value (in $L(\mathbb{R}^3, \mathbb{R}^3)$), rather than differentiation with respect to the spatial domain of the image ($\mathbb{R}^3$). The tensor-valued gradient of a scalar invariant J is notated here with $\boldsymbol{\nabla} J$ (rather than ∇J):

$$\boldsymbol{\nabla} J : L(\mathbb{R}^3, \mathbb{R}^3) \mapsto L(\mathbb{R}^3, \mathbb{R}^3) \; ; \; \boldsymbol{\nabla} J = \frac{\partial J}{\partial \mathbf{D}} \; ; \; ([\boldsymbol{\nabla} J]_{\mathcal{L}})_{ij} = \frac{\partial J}{\partial D_{ij}}$$

By differentiating the spectral decomposition (12.10), one finds $\boldsymbol{\nabla}\lambda_i = \mathbf{e}_i \otimes \mathbf{e}_i$, and thus $\boldsymbol{\nabla}\lambda_i : \boldsymbol{\nabla}\lambda_j = \delta_{ij}$. That is, $\{\boldsymbol{\nabla}\lambda_1, \boldsymbol{\nabla}\lambda_2, \boldsymbol{\nabla}\lambda_3\}$ is an orthonormal basis for shape change around a given tensor value. However, this basis lacks the immediate anatomical significance associated with the eigenvalue statistics (described in the previous section), and the gradients of sorted eigenvalues are not defined when two or more eigenvalues are equal.

To address this, an alternative orthonormal basis for shape change is proposed, based on the (tensor-valued) gradients of μ_1, μ_2, and α_3. From the

first-order Taylor expansion of J around $\mathbf{D}$, $J(\mathbf{D}+\boldsymbol{\epsilon}) = J(\mathbf{D})+\boldsymbol{\epsilon}:\boldsymbol{\nabla}J+O(\boldsymbol{\epsilon}^2)$, the gradients of the J_i invariants can be computed as [2]:

$$\begin{array}{ll} \boldsymbol{\nabla}J_1(\mathbf{D}) = \mathbf{I} & \boldsymbol{\nabla}J_2(\mathbf{D}) = \mathrm{tr}(\mathbf{D})\mathbf{I} - \mathbf{D} \\ \boldsymbol{\nabla}J_3(\mathbf{D}) = \det(\mathbf{D})\mathbf{D}^{-1} & \boldsymbol{\nabla}J_4(\mathbf{D}) = 2\mathbf{D} \end{array} \tag{12.11}$$

Expressions for $\boldsymbol{\nabla}\mu_1$, $\boldsymbol{\nabla}\mu_2$, and $\boldsymbol{\nabla}\alpha_3$ may then be built up from (12.4), (12.6), (12.7), and (12.11), using the standard rules of vector calculus. The spectral decomposition (12.10) allows the double contraction of the gradients of invariants J and K to be reduced to a simple three-dimensional vector dot product:

$$\begin{aligned} \boldsymbol{\nabla}J:\boldsymbol{\nabla}K &= (\textstyle\sum_i \partial J/\partial\lambda_i\ \mathbf{e}_i\otimes\mathbf{e}_i):(\sum_j \partial K/\partial\lambda_j\ \mathbf{e}_j\otimes\mathbf{e}_j) \\ &= \textstyle\sum_{i,j}(\partial J/\partial\lambda_i)(\partial K/\partial\lambda_j)\delta_{ij} \\ &= \textstyle\sum_i(\partial J/\partial\lambda_i)(\partial K/\partial\lambda_i) \\ &= \nabla_\lambda J\cdot\nabla_\lambda K \end{aligned}$$

Then, (12.8) establishes the mutual orthogonality of $\boldsymbol{\nabla}\mu_1$, $\boldsymbol{\nabla}\mu_2$, and $\boldsymbol{\nabla}\alpha_3$.

Where defined, the eigenvalue gradients $\boldsymbol{\nabla}\lambda_i$ have constant unit magnitude. $\|\widehat{\boldsymbol{\nabla}}\mu_1\| = 1/3$ is also constant, but the gradients of μ_2 and α_3 have varying magnitude, because their ranges are bounded. $\boldsymbol{\nabla}\mu_2$ vanishes when all eigenvalues are equal (μ_2 at minimum), and $\boldsymbol{\nabla}\alpha_3$ vanishes when two eigenvalues are equal (α_3 at extremum). Still, the space of shape changes is always three-dimensional, so some scheme is required to 'fix' the $\{\boldsymbol{\nabla}\mu_1, \boldsymbol{\nabla}\mu_2, \boldsymbol{\nabla}\alpha_3\}$ basis to consistently span the space of shape variation. Developing this scheme is a focus of ongoing work. One inelegant approach is to, at each tensor sample in an image being processed, slightly perturb the tensor values if there is equality between eigenvalues, so that $\boldsymbol{\nabla}\mu_2$ and $\boldsymbol{\nabla}\alpha_3$ become non-zero.

Normalized invariant gradients are then defined by:

$$\widehat{\boldsymbol{\nabla}}J = \boldsymbol{\nabla}J/\|\boldsymbol{\nabla}J\|\ ;\ J = \mu_1, \mu_2, \alpha_3$$

12.6 Application to Diffusion Tensor Images

The tensor field is assumed to be a continuous and differentiable function $\mathbf{D}: \mathbb{R}^3 \mapsto Sym_3$, as is ensured by the band-limited nature of MRI measurements. The gradient of $\mathbf{D}$ is a *third-order* tensor, described by Pajevic et al. [20]:

$$\nabla\mathbf{D} : \mathbb{R}^3 \mapsto Sym_3^3\ ;\ \nabla\mathbf{D} = \frac{\partial\mathbf{D}}{\partial\mathbf{x}}\ ;\ ([\nabla\mathbf{D}]_{\mathcal{L}})_{ijk} = \frac{\partial D_{ij}}{\partial x_k}$$

The double contraction of a second-order tensor with a third-order tensor is a first-order tensor – a vector. Double contracting invariant gradient $\boldsymbol{\nabla}J$ with field gradient $\nabla\mathbf{D}$ creates a vector ∇J, measuring spatial changes of J in the tensor field $\mathbf{D}$. This is simply the chain rule applied to $J(\mathbf{D}(\mathbf{x}))$:

$$\nabla J : \mathbb{R}^3 \mapsto \mathbb{R}^3\ ;\ \nabla J(\mathbf{x}) = \boldsymbol{\nabla}J(\mathbf{D}(\mathbf{x})):\nabla\mathbf{D}(\mathbf{x})\ ;\ ([\nabla J(\mathbf{x})]_{\mathcal{L}})_k = \sum_{i,j}\frac{\partial J}{\partial D_{ij}}\frac{\partial D_{ij}}{\partial x_k}$$

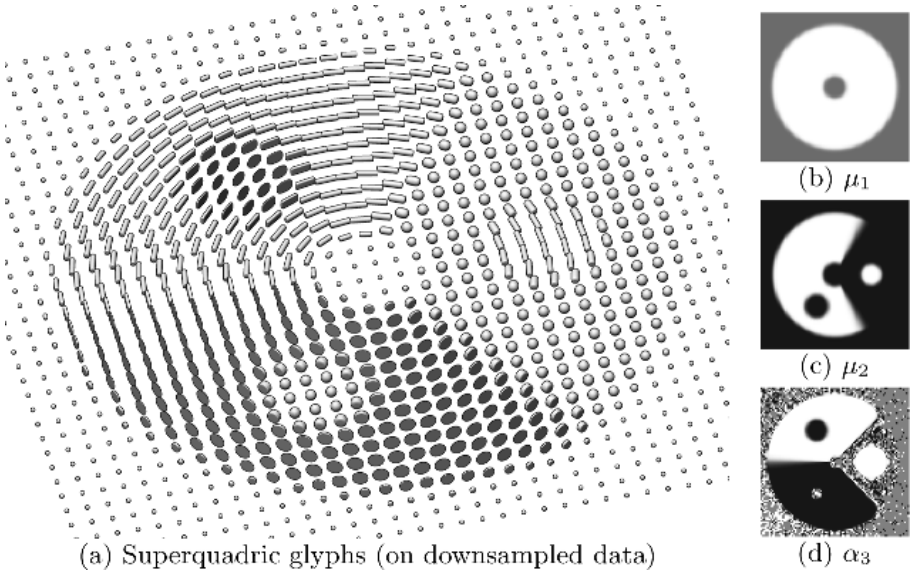

Fig. 12.3. Synthetic tensor image for testing gradient measures. Superquadric glyphs are shown in (**a**). Eigenvalue statistics are shown in grayscale in (**b**), (**c**), and (**d**)

Note that $|\nabla J|$ is effectively scaled by $\|\boldsymbol{\nabla} J\|$. This has implications for how spatial changes (edges) in shape are detected. Because $\|\boldsymbol{\nabla}\lambda_i\| = 1$, the spatial eigenvalue gradients $\nabla\lambda_i$ will collectively indicate any and all shape changes in a tensor field, while $\nabla\mu_2$ and $\nabla\alpha_3$ fail in this respect. For example, $\nabla\mu_2$ does not detect changes in anisotropy around a field location with an isotropic tensor. This motivated the definition of $\{\widehat{\boldsymbol{\nabla}}\mu_1, \widehat{\boldsymbol{\nabla}}\mu_2, \widehat{\boldsymbol{\nabla}}\alpha_3\}$ – an *anatomically relevant* orthonormal basis for tensor shape change. With this in mind, a novel 'equi-sensitive' spatial gradient of invariant J is defined as:

$$\nabla J : \mathbb{R}^3 \mapsto \mathbb{R}^3 \; ; \; \nabla J(\mathbf{x}) = \widehat{\boldsymbol{\nabla}} J(\mathbf{D}(\mathbf{x})) : \nabla \mathbf{D}(\mathbf{x})$$

Note that $\nabla J \neq \nabla J/|\nabla J|$. Rather, $\nabla J = \nabla J/\|\boldsymbol{\nabla} J\|$, assuming $\|\boldsymbol{\nabla} J\| > 0$.

The spatial gradients are demonstrated with a two-dimensional synthetic dataset shown in Fig. 12.3. There are four types of materials (isotropic low diffusivity, isotropic high diffusivity, planar anisotropic, and linear anisotropic), with boundaries between every material pair. Eigenvalue statistics are evaluated at each tensor sample and shown in Figs. 12.3(b), 12.3(c), and 12.3(d). The gradient measurement results are shown in Fig. 12.4. Figure 12.4(a) shows a measure of both shape and orientation gradients, $\|\nabla \mathbf{D}\| = \sqrt{\sum_{ijk}(\partial D_{ij}/\partial x_k)^2}$ [20]. However, note that Figs. 12.4(b) and 12.4(c) indicate shape changes only, and with equal sensitivity, as intended. Finally, Figs. 12.4(d), 12.4(e), and 12.4(f) show how the edges in the three degrees of freedom in shape can be detected in isolation.

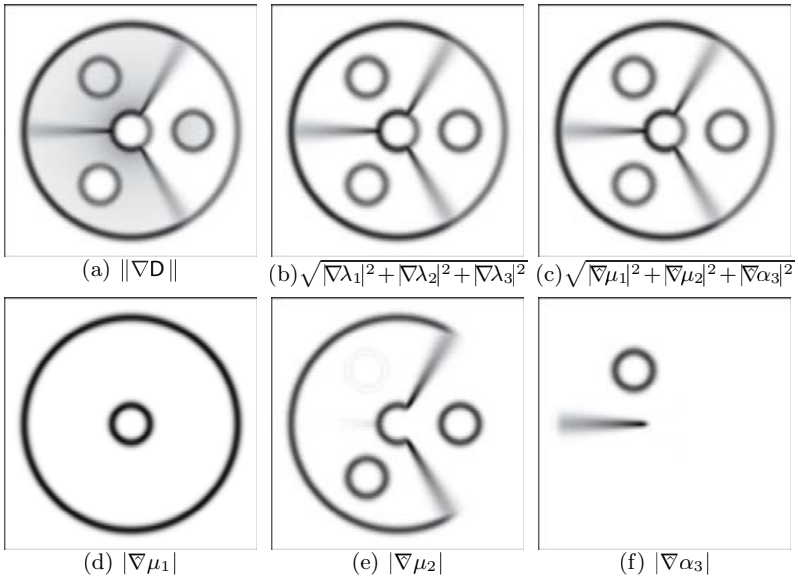

Fig. 12.4. Gradient magnitudes of synthetic data, shown with inverted grayscale

12.7 Discussion

This chapter describes a method for detecting changes (edges) in tensor shape within diffusion tensor fields. A particular set of three tensor invariants (the eigenvalue statistics μ_1, μ_2, α_3) was leveraged for both its orthogonality and its relevance to anatomical feature detection. Tensor analysis was used to create a tensor-valued orthonormal basis for shape change, against which the spatial gradient of the tensor field is measured. Various aspects of this work require further development, most importantly the robust and efficient computation of the invariant-based orthonormal basis for shape change, since this must be calculated anew at every tensor value. Ongoing work is validating the utility of this approach on real data, as well as assessing the impact of noise in the MRI measurements. In the interests of space, the practical details of efficiently measuring the derivatives of the tensor components (for $\nabla\mathbf{D}$) have not been explored here, though continuous tensor field models from convolution or splines (see Chap. 18) provide a natural basis for this.

References

1. PJ Basser, J Mattiello, and D Le Bihan. Estimation of the effective self-diffusion tensor from the NMR spin-echo. *Journal of Magnetic Resonance, B*, 103(3):247–254, 1994.
2. GA Holzapfel. *Nonlinear Solid Mechanics*, Chap. 1. John Wiley and Sons, Ltd, England, 2000.

3. AM Uluğ and PCM van Zijl. Orientation-independent diffusion imaging without tensor diagonalization: Anisotropy definitions based on physical attributes of the diffusion ellipsoid. *Journal of Magnetic Resonance Imaging*, 9:804–813, 1999.
4. KM Hasan, PJ Basser, DL Parker, and AL Alexander. Analytical computation of the eigenvalues and eigenvectors in DT-MRI. *Journal of Magnetic Resonance*, 152:41–47, 2001.
5. EW Weisstein. *CRC Concise Encyclopedia of Mathematics*, pp. 362–365, 1652. CRC Press, Florida, 1999.
6. WH Press, BP Flannery, SA Teukolsky, and WT Vetterling. *Numerical Recipes: The Art of Scientific Computing*. Cambridge University Press, Cambridge (UK) and New York, 2nd edition, 1992.
7. RWD Nickalls. A new approach to solving the cubic: Cardan's solution revealed. *The Mathematical Gazette*, 77:354–359, November 1993.
8. MM Bahn. Invariant and orthonormal scalar measures derived from magnetic resonance diffusion tensor imaging. *Journal of Magnetic Resonance*, 141:68–77, 1999.
9. JC Criscione, JD Humphrey, AS Douglas, and WC Hunter. An invariant basis for natural strain which yields orthogonal stress response terms in isotropic hyperelasticity. *Journal of Mechanics and Physics of Solids*, 48:2445–2465, 2000.
10. G Kindlmann. Superquadric tensor glyphs. In *Proceedings IEEE TVCG/EG Symposium on Visualization 2004*, pp. 147–154, May 2004.
11. PJ Basser and DK Jones. Diffusion-tensor MRI: theory, experimental design and data analysis – a technical review. *Nuclear Magnetic Resonance in Biomedicine*, 15:456–467, 2002.
12. C Pierpaoli, P Jezzard, PJ Basser, A Barnett, and G DiChiro. Diffusion tensor MR imaging of the human brain. *Radiology*, 201(3):637–648, 1996.
13. AM Uluğ, N Beauchamp, RN Bryan, and PCM van Zijl. Absolute quantitation of diffusion constants in human stroke. *Stroke*, 28(3):483–490, 1997.
14. C Beaulieu. The basis of anisotropic water diffusion in the nervous system – a technical review. *Nuclear Magnetic Resonance in Biomedicine*, 15:435–455, 2002.
15. C Pierpaoli and PJ Basser. Toward a quantitative assessment of diffusion anisotropy. *Magnetic Resonance in Medecine*, 33:893–906, 1996.
16. DC Alexander, GJ Barker, and SR Arridge. Detection and modeling of non-gaussian apparent diffusion coefficients profiles in human brain data. *Magnetic Resonance in Medecine*, 48:331–340, 2002.
17. AL Alexander, KM Hasan, M Lazar, JS Tsuruda, and DL Parker. Analysis of partial volume effects in diffusion-tensor MRI. *Magnetic Resonance in Medicine*, 45:770–780, 2001.
18. MR Wiegell, HBW Larsson, and VJ Wedeen. Fiber crossing in human brain depicted with diffusion tensor MR imaging. *Radiology*, 217(3):897–903, Dec 2000.
19. DS Tuch, RM Weisskoff, JW Belliveau, and VJ Wedeen. High angular resolution diffusion imaging of the human brain. In *Proceedings 7th Annual Meeting of ISMRM*, page 321, 1999.
20. S Pajevic, A Aldroubi, and PJ Basser. A continuous tensor field approximation of discrete DT-MRI data for extracting microstructural and architectural features of tissue. *Journal of Magnetic Resonance*, 154:85–100, 2002.
21. K Hoffman and R Kunze. *Linear Algebra*. Prentice-Hall, Inc., Englewood Cliffs, NJ, 1971.